PERGAMON

Computers and Structures 77 (2000) 735–745

Computers & Structures

www.elsevier.com/locate/compstruc

A study of loading history effect for thermoviscoelastic solid propellant grains

Shiang-Woei Chyuan [a,b,*]

[a] Department of Mechanical Engineering, National Taiwan University, Taipei, Taiwan, ROC
[b] Chung Shan Institute of Science and Technology, Lung-Tan, Tao-Yuan 325, P.O. Box 90008-15-3, Taiwan, ROC

Received 7 January 1999; accepted 18 November 1999

Abstract

The results of an investigation on solid propellant grains considering loading history effect are presented. Traditionally, the thermal loading history effect of solid propellant grains was not considered for simplifying the analytical task, and a higher safety factor was inevitable for structural integrity. But this does not mean that the thermal loading history effect is not useful and could be neglected arbitrarily, and this effect usually plays a very important role for some critical design. In order to simulate the time–temperature-dependent behavior of thermoviscoelastic and incompressible polymer materials, concepts of time–temperature shift principle, cumulative damage theory and reduced integration were used. In addition, five different types of thermal loading history assumption were performed using the finite element method for discussing the thermal loading history effect. Results show that the thermal loading history effect is important for structural integrity of solid propellant grains, and improper negligence may cause structural failure of missile systems.

Keywords: Shift factor; Reduced time; Loading history; Cumulative damage; Relaxation modulus; Thermoviscoelastic; Finite element method

1. Introduction

Solid rocket motor structural design is currently based on the concept of a mechanically weak solid propellant grain, cast into a stronger metallic or composite case. The outer case provides the essential structural resistance against service and operational loads, and the inner propellant grain's low strength is used for the transmission of loads from the grain surface to the outer case. In general, solid rocket motors are subjected to diverse loadings during shipment, storage and firing. It is well known that under these loading conditions, cracks can develop in solid propellants because of excessive loads. Therefore, in order to determine the integrity and the ultimate service life of solid rocket motors, studies should be conducted to evaluate the significance of the value and distribution of stress and strain.

In a missile system, the structural configuration of solid rocket motor is one of the most complicated parts, and numerical techniques are necessary to simulate the physical behavior and to evaluate the structural integrity of the different design, and to minimize the cost of product development. During the last two decades, more and more attention has been paid to the design, manufacturing, and evaluation of solid propellant grains in order to meet service life and performance requirements [1]. Meanwhile, it is also recognized that aging studies (e.g. mechanical aging [2,3], chemical aging [4,5], etc.) are extremely necessary to predict the service life of solid propellant grains, and the thermal response under thermal shock loads [6] plays an important role. Therefore, the reduction of thermal response is one of the significant considerations in the primary design of solid propellant grains and some effective designs (e.g. free flap design, P-groove design, stress reliever

* Address: Chung Shan Institute of Science and Technology, Lung-Tan, Tao-Yuan 325, P.O. Box 90008-15-3, Taiwan, ROC.
E-mail address: yeaing@iris.seed.net.tw (S.-W. Chyuan).

0045-7949/00/$ - see front matter
PII: S0045-7949(00)00009-2

design, etc.) have been adopted [7]. For the time–temperature-dependent behavior of thermoviscoelastic and incompressible polymer materials, the concept of time–temperature shift principle, reduced integration and thermorheologically simple material (TSM) assumption were widely used in the linear viscoelastic analysis [8–10]. In addition, the method of nonlinear viscoelastic analysis of solid propellant grains for ignition pressurization load was developed following a step-by-step finite element simulation, considering the material and geometrical non-linearities due to the nonlinear bulk modulus [11]. Because the thermal loading history effect of solid propellant grains was not considered for simplifying the analytical task in the past literature [1–11], the time–temperature-dependent behavior of incompressible and viscoelastic polymer materials cannot be simulated and modeled accurately. In order to study the thermal loading history effect, application of cumulative damage theory [12,13] and five different types of thermal loading history assumption were used in this article. A successful and feasible numerical model following a step-by-step thermal loading history was used and discussed thoroughly in this article.

From the above statements concerning solid propellant grains, one can see that it is a very difficult and laborious task to predict the physical response during the design phase. Therefore, the use of a computer simulation technique to analyze the structural behavior of solid rocket motor in the preliminary design stage is very important and necessary. Among different numerical approaches, the finite element method (FEM) [14,15] and the boundary element method (BEM) [16]; and the increasing developments of digital computer power have moved from being research tools for select groups to become powerful design tools for engineers. For problems with singularities (e.g. seepage flow problems, crack, etc.), it is well known that BEM accompanying dual integral formulation [17] became a very effective analytical model. However, the main drawback of BEM is that it is not easy to apply in the field of complicated design. Therefore, FEM has become the most widely used numerical technique for solid propellant grains, because the extremely complex structural configurations (e.g. cylinder head structure [18]) can be modeled using finite elements and the response at any desired point of the structure can be easily determined [19].

2. Finite element modeling

2.1. Constitutive model and material properties of solid propellant grains

All modern solid propellant grains utilize an elastomeric binder, which is filled with quite high levels of solid particles. The application of a load causes different mechanisms to take place in the binder, the filler or the interface between them, such as the breakage of polymer chains, breakage and reformation of weak bonds, deformation and geometrical rearrangement of filler particles, interfacial debonding, also called dewetting, the formation of microvoids at or near the interface of the particles and surrounding matrix. Under these influences, solid propellant grains exhibit very complex behavior, including features associated with time and rate effects, temperature and superimposed pressure dependence, large deformations and large strains, stress softening during cyclic loading, and transition from incompressible to compressible behavior. Therefore, an attempt to represent all aspects of solid propellant grain behavior would result in a very complicated constitutive model and would require a wide range of tests to characterize the propellant grains. Thus, a number of previous investigations have been concerned with certain features only. In the present article, a proper constitutive model [20,21] of solid propellant grains for engineering analysis was used.

$$\sigma(t) = \int_0^t \{E(t-\tau)[\partial\varepsilon(t)/\partial\tau]\}\,\mathrm{d}\tau, \tag{1}$$

where $\sigma(t)$ is the stress relaxation function, and $E(t)$ is the relaxation modulus. The dependence of the viscoelastic properties on the temperature is introduced in the form of an assumption that the solid propellant grain is a rheologically simple material. This assumption permits the introduction of reduced time ξ, which is defined as follows [22]:

$$\xi = \int_0^t \{\mathrm{d}\tau'/a_T\}, \tag{2}$$

where a_T is the time–temperature shift function. The consequence of the existence of the reduced time is that a viscoelastic property at some arbitrary temperature T can now be related to the same function at some reference temperature T_0; e.g.,

$$E(T,t) = E(T_0,\xi). \tag{3}$$

The effective propellant modulus, E_{eq}, to be used in the stress and strain analysis, shall be obtained from the master relaxation modulus curve at a temperature-reduced time corresponding to the time required to reach equilibrium, t^*, divided by the shift factor, a_T, for the surrounding temperature; i.e.,

$$E_{\mathrm{eq}} = E(t^*/a_t). \tag{4}$$

For the (hydroxy terminated polybutadiene binder) propellant used in this analysis, the relaxation modulus versus the temperature-reduced time is shown in Fig. 1, and the time-shift factor for the HTPB propellant is shown in Fig. 2. The curves in Figs. 1 and 2 are plotted

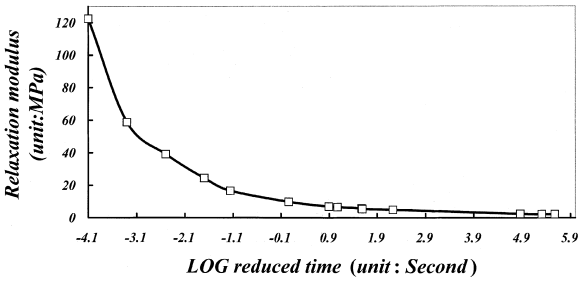

Fig. 1. The master curve of the relaxation modulus for the HTPB propellant (reference temperature: +25°C).

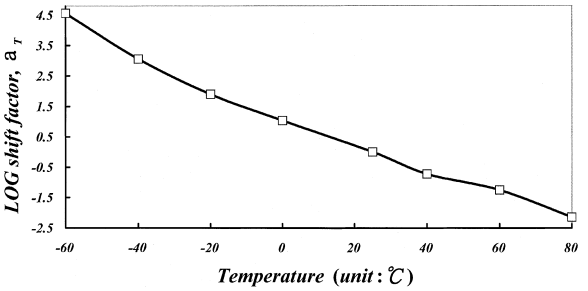

Fig. 2. The time-shift factor for the HTPB propellant (reference temperature: +25°C).

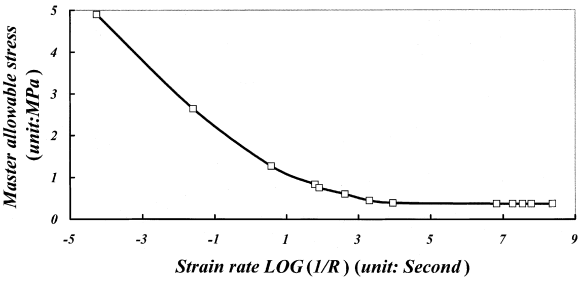

Fig. 3. The master curve of the allowable stress for the HTPB propellant (reference temperature: +25°C).

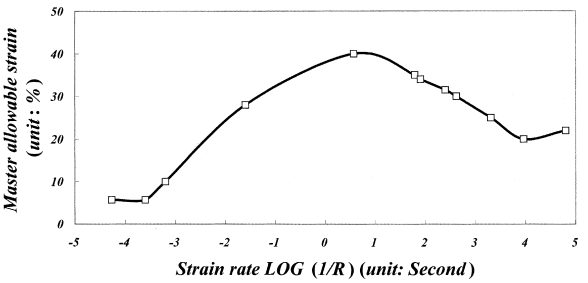

Fig. 4. The master curve of the allowable strain for the HTPB propellant (reference temperature: +25°C).

according to the experimental data in the environment under different temperatures. Propellant failure properties shall be used on master curves of maximum nominal stress, σ_{max}, and strain at maximum nominal stress, ε_{max}, versus temperature-reduced time, t/a_T. The tests used to generate these master curves will be conducted in accordance with the JANNAF tentative standard uniaxial test procedure and at the same temperatures for which, relaxation modulus tests were conducted in Ref. [23]. The time–temperature shift factor, a_T, obtained from the relaxation modulus tests shall be utilized in constructing the master uniaxial failure curves. The failure criterion for the solid propellant grains depends on its allowable stress and allowable strain, and the strength of the HTPB propellant used in this article is obtained from the master allowable stress and allowable strain curve in Figs. 3 and 4. The curves in Figs. 3 and 4 are also plotted according to the experimental data in the environment under different temperatures. In addition, Poisson's ratio (v_p) and the coefficient of linear thermal expansion (α_p) for the HTPB propellant from Ref. [23] were used in the stress and strain analysis, and Poisson's ratio (v_i) and coefficient of linear thermal expansion (α_i) for the liner between the outer steel case and the inner propellant grains from [23] were adopted. The reference temperature, T_{SF}, for strain-free and stress-free condition, will be taken to be 20°F above the propellant cure temperature, T_{cure}, for solid rocket motors, which are not pressure cured. Young's modulus (E_c), Poisson's ratio (v_c) and thermal expansion coefficient (α_c) for the outer steel case from Ref. [23] were used in this work.

2.2. Finite element modeling of solid rocket motor and reduced integration

Because of the complexity of geometrical design and load path of a solid rocket motor system, it is not easy to model the complicated stiffness distribution of this structure, just using a simple analytical model. Therefore, a 3D solid model was chosen for this structure in order to predict the stress and strain response in detail. The density on some critical areas is much higher than other sub-critical parts in order to reduce the number of degrees of freedom. Due to the symmetry of the geometry and loading, a model of a five-degree segment with axis-symmetric boundary conditions on the cut faces was utilized for simplicity without loss of accuracy. Some appropriate finite element mesh (Fig. 5) with 1408 eight-node solid elements (CHEXA) [24,25] and 2956 grid nodes were built for the stress and strain analysis, respectively, to acquire their corresponding convergent results. As Poisson's ratio v approaches 0.5, the material becomes incompressible. For convenience, it is tempting to approximate incompressibility by using $v = 0.49$. But, near $v = 0.5$, stresses are strongly dependent on v, stresses may double as v goes from 0.48 to 0.50. Also,

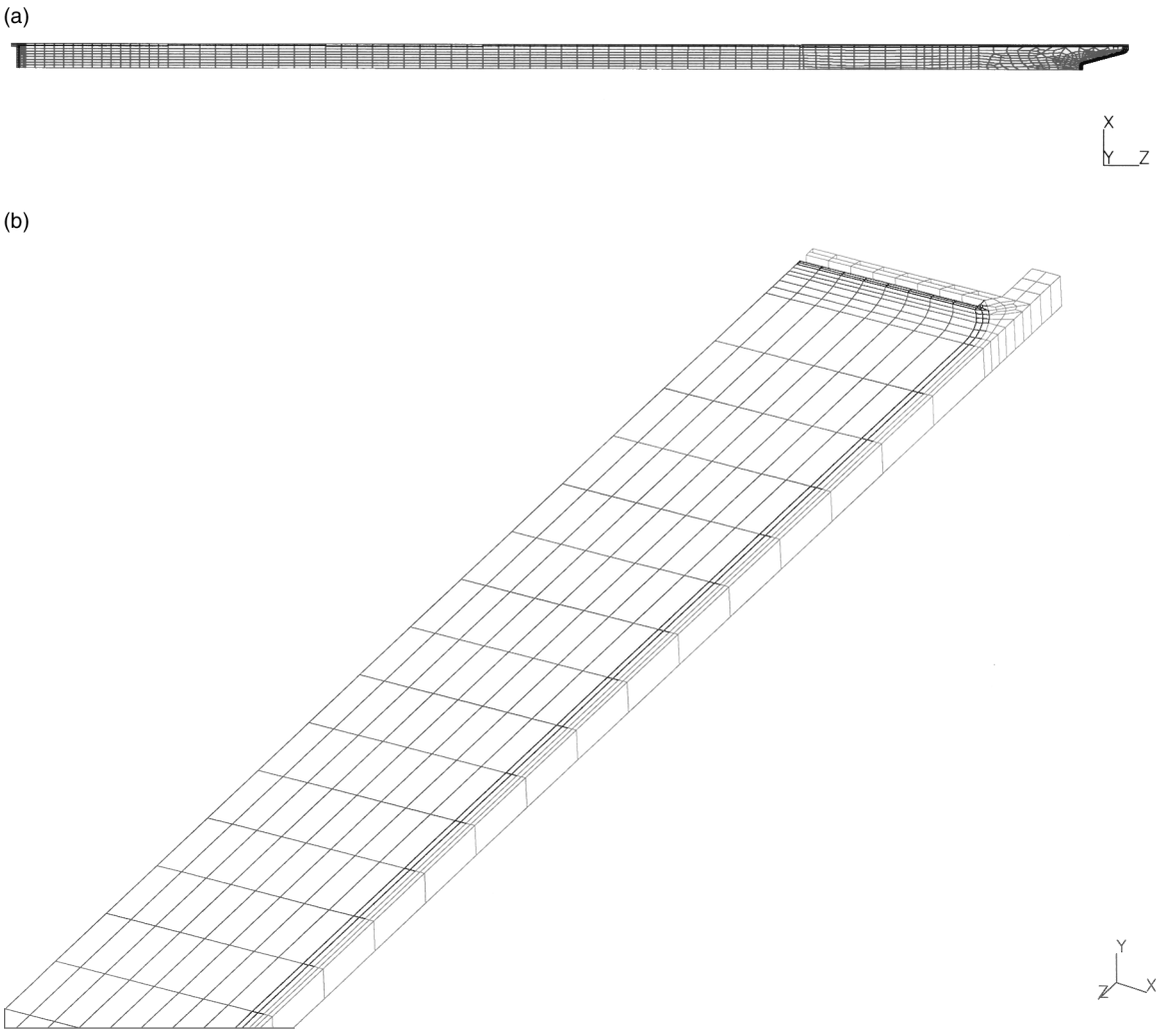

Fig. 5. (a) The finite element model of a solid rocket motor and (b) the local model of a solid rocket motor.

structural equations become ill-conditioned as v approaches 0.5 and numerical instability becomes more likely, and finally the mesh "locks". In this article, reduced integration [14] was adopted to simulate the nearly incompressible property of the solid propellant grains. In addition, the finite element analysis was executed on an IBM590/RS6000 computer system, and the CPU time for a static run, under a single load step case was 57.14 s. If a personal computer (PC) system with a Pentium Pro 200 processor was used, the CPU time required for a static run under a single load step case was 32.53 s.

2.3. Failure criteria of solid propellant grains

In general, the critical location under an ignition pressurization loading case is at the interface between the outer case and the inner HTPB propellant, and the critical location under thermal loading case is at the inner bore free surface of solid propellant grains. Because the main aim of this article is to study the thermal loading history effect, the maximum principal strain (ε_{max}) of the inner bore free surface of solid propellant grains was chosen to be analyzed and discussed. From JANNAF Solid Propellant Structural Integrity Handbook [23], the maximum principal stress failure criterion for thermal loading case, expressed in terms of strain, shall be used for evaluating structural failures:

$$\varepsilon_{\text{allowable,max}} = (1-v^2)^* \varepsilon_{\text{measured,max}}(t^*/a_T), \tag{5}$$

where $\varepsilon_{\text{measured,max}}(t^*/a_T)$ is the allowable uniaxial strain as determined from the master uniaxial strain at maximum nominal stress versus t^*/a_T curve evaluated at the time to reach thermal equilibrium, t^*.

2.4. Cumulative damage theory of solid propellant grains

The first cumulative damage theory was proposed by Palmgren in 1924 and later developed by Miner in 1945 [12], which is still widely used, is referred to as the Palmgren–Miner hypotheses or the linear damage rule. By the definition of Ref. [12], operation at a constant stress amplitude S_1 will produce complete damage, or failure, in N_1 cycles. Operation at a stress amplitude S_1 for a number of cycles n_1 smaller than N_1 will produce a smaller fraction of damage, say D_1, usually termed the damage fraction. Operation over a spectrum of diverse stress levels results in a damage fraction D_i for each of the different stress levels S_i in the spectrum. When these damage fractions sum to unit, failure is predicted; i.e.

$$\begin{aligned}\sum D_i &= D_1 + D_2 + D_3 + \cdots + D_{m-1} + D_m \\ &= n_1/N_1 + n_2/N_2 + n_3/N_3 + \cdots \\ &\quad + n_{m-1}/N_{m-1} + n_m/N_m \\ &= \sum n_i/N_i \geqslant 1. \end{aligned} \tag{6}$$

The Palmgren–Miner hypotheses asserts that the damage fraction at any stress level S_i is linearly proportional to the ratio of the number of cycles of operation to the total number of cycles that would produce failure at that stress level. For solid propellant grains, the cumulative damage theory will be used to calculate the factor of safety (SF), under diverse thermal loading history assumption.

$$\mathrm{SF}_{\varepsilon} = 1/D_{\varepsilon} = \varepsilon_{\mathrm{allowable,max}}/\varepsilon_{\max}, \tag{7}$$

where $\varepsilon_{\max}$ is the maximum principal strain from the thermal strain analysis results.

$$(1/\mathrm{SF})_{\varepsilon} = D_{\varepsilon} = \sum D_{i,\varepsilon} = \sum(\Delta\varepsilon_i/\varepsilon_f), \tag{8}$$

where D_{ε} is the damage fraction with respect to the thermal strain analysis results. In addition, ε_{f} is the allowable strain of the HTPB propellant, and $\Delta\varepsilon_{\mathrm{i}}$ is the increment of the thermal strain under the ith load step of the diverse thermal loading history.

3. Thermal loading history of solid rocket motor system

For a missile system, the reference temperature, T_{SF}, for a strain-free and stress-free condition, shall be taken to be 20°F above the propellant cure temperature (T_{cure}) for motors which are not pressure cured, and the solid rocket motor will be placed at the storage temperature T_{storage} (e.g. +25°C) during the period time of t_{cooldown} (e.g. five days) for thermal cooldown to equilibrium. After a long period of t_{storage} ($t_{\mathrm{storage}} \gg t_{\mathrm{cooldown}}$; e.g. 40 days) for storage, the motor will be taken to be placed at the lowest (firing) temperature T_{firing}, during a shorter period of t_{firing} (e.g. 60 min; $t_{\mathrm{storage}} \gg t_{\mathrm{cooldown}} > t_{\mathrm{firing}}$), and the motor will be used in the static test (firing). If the storage time t_{storage} is higher, the chemical aging and the creep behavior need to be considered. In this article, the effect of aging and creep was ignored for simplifying the laborious analytical task. Therefore, the surrounding temperature diagram of a solid rocket motor from curing through storage to static test (firing) could be shown in Fig. 6. In addition, five different thermal loading history assumptions were chosen, analyzed and discussed.

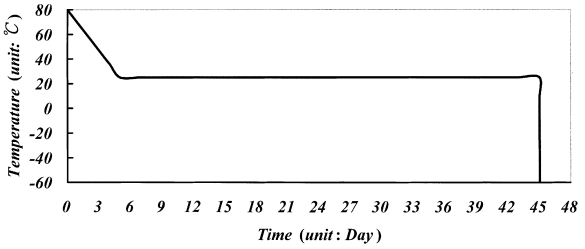

Fig. 6. The surrounding temperature diagram of a solid rocket motor.

3.1. Thermal loading history assumption 1

The design load is defined as $T_{\mathrm{design}} = (T_{\mathrm{firing}} - T_{\mathrm{SF}})$, $T_{\mathrm{SF}} = +80°\mathrm{C}$, $T_{\mathrm{firing}} = -60°\mathrm{C}$; $t_{\mathrm{cooldown}} = 5$ days, $t_{\mathrm{firing}} = 60$ min; $T_{\mathrm{storage}} = +25°\mathrm{C}$; just one load step along the total thermal loading history. In this condition, the material properties of solid propellant grains are invariant during the load step, and the loading history effect between T_{SF} and T_{firing} is ignored like the past literature [1–11].

3.2. Thermal loading history assumption 2

$T_{\mathrm{SF}} = +80°\mathrm{C}$, $T_{\mathrm{firing}} = -60°\mathrm{C}$; $t_{\mathrm{cooldown}} = 5$ days, $t_{\mathrm{firing}} = 60$ min; $T_{\mathrm{storage}} = +25°\mathrm{C}$; one thermal load step from curing to storage and one thermal load step from storage to static test (firing), and totally two thermal load steps along the total thermal loading history. In this condition, the material properties are different in these two load steps, and the loading history effect between T_{SF} and T_{firing} is considered using two thermal load steps for an approximate result.

3.3. Thermal loading history assumption 3

$T_{\mathrm{SF}} = +80°\mathrm{C}$, $T_{\mathrm{firing}} = -60°\mathrm{C}$; $t_{\mathrm{cooldown}} = 5$ days, $t_{\mathrm{firing}} = 60$ min; $T_{\mathrm{storage}} = +25°\mathrm{C}$; five thermal load steps from curing to storage and five thermal load steps from storage to firing, and totally 10 thermal load steps along the total thermal loading history. Under this condition, the material properties are variant in these 10 load steps, and the loading history effect between T_{SF} and T_{firing} is

considered using 10 thermal load steps for a better result.

3.4. Thermal loading history assumption 4

$T_{SF} = +80°C, T_{firing} = -60°C; t_{cooldown} = 5$ days, $t_{firing} = 60$ min; $T_{storage} = +25°C$; 10 thermal load steps from curing to storage and 10 thermal load steps from storage to firing, and totally 20 thermal load steps along the total thermal loading history. In this condition, the material properties are variant in these 20 load steps, and the loading history effect between T_{SF} and T_{firing} is considered using 20 thermal load steps for a good result.

3.5. Thermal loading history assumption 5

$T_{SF} = +80°C, T_{firing} = -60°C; t_{cooldown} = 5$ days, $t_{firing} = 60$ min; $T_{storage} = +25°C$; 20 thermal load steps from curing to storage and 20 thermal load steps from storage to firing, and totally 40 thermal load steps along the total thermal loading history. In this condition, the material properties are variant in these 40 load steps, and the loading history effect between T_{SF} and T_{firing} is considered using 40 thermal load steps for the best result.

4. Finite element analysis

4.1. Thermal loading history assumption 1

Under this thermal loading condition, the design load is defined as $T_{design} = (T_{firing} - T_{SF}) = -140°C$. The effective propellant modulus ($E_{eq} = E(t^*/a_T) = 6.566$ MPa) could be obtained from Fig. 1, and the shift factor ($\log a_T = 4.6$) could be obtained from Fig. 2. From the finite element simulation, the maximum effective stress ($\sigma_{eff,\Delta T}$) of outer case is 1.85 kgf/mm^2 ($= 18.13$ MPa) (Fig. 7), the maximum principal stress ($\sigma_{max,\Delta T}$) of HTPB propellant is 0.129 kgf/mm^2 ($= 1.264$ MPa) (Fig. 8), the maximum shear stress ($\tau_{max,\Delta T}$) of propellant is 0.0613 kgf/mm^2 ($= 0.601$ MPa) (Fig. 9), the maximum principal strain ($\varepsilon_{max,\Delta T}$) of the propellant is 11.4% (Fig. 10), and the critical area is located at the inner bore free surface of solid propellant grains. Using the time–temperature shift principle, the reciprocal value of the reduced strain rate (R) could be calculated.

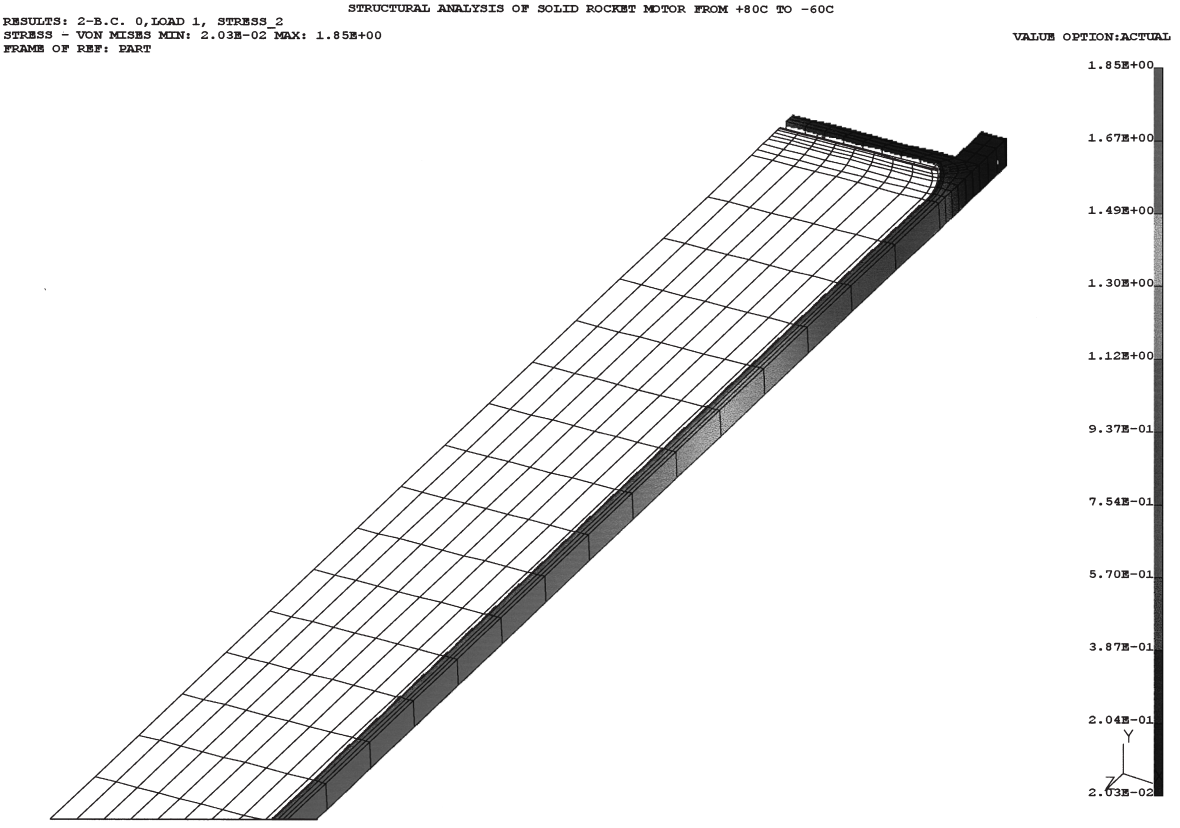

Fig. 7. The maximum effective stress distribution of the outer case under thermal loading history assumption 1 case.

$$\log(1/R) = \log(t/\varepsilon_{\max}) - \log a_T = +1.91.$$

Inserting the value of $\log(1/R)$ in Fig. 4, the value of $\varepsilon_{\text{measured,max}}(t^*/a_T)$ could be found. From Eq. (5), the maximum allowable strain could be calculated:

$$\varepsilon_{\text{allowable,max}} = (1-\nu^2)^* \varepsilon_{\text{measured,max}}(t^*/a_T) = 24.8\%.$$

Then, inserting the value of $\varepsilon_{\text{allowable,max}}$ in Eq. (7), the factor of safety or damage fraction with respect to the strain result could be calculated:

$$\begin{aligned} \text{SF}_{\varepsilon,\Delta T} &= 1/D_{\varepsilon,\Delta T} = \varepsilon_{\text{allowable,max}}/\varepsilon_{\max,\Delta T} = 2.175 \\ &= 1/0.460. \end{aligned} \tag{9}$$

Using Eq. (8), the final factor of safety (SF) or damage fraction (D), located at the inner bore free surface of the HTPB propellant under thermal loading history assumption 1 could be calculated from the results of Eq. (9).

$$\begin{aligned} (1/\text{SF})_{\varepsilon} &= D_{\varepsilon} = \sum D_{i,\varepsilon} = D_{\varepsilon,\Delta T} = 0.460 \\ &= 1/2.175. \end{aligned} \tag{10}$$

4.2. Thermal loading history assumption 2

4.2.1. The load step from $T_{SF} = +80^\circ C$ to $T_{storage} = +25^\circ C$

Under this thermal loading condition, the design load is defined as $T_{\text{design}} = -55°\text{C}$. The effective propellant modulus ($E(t^*/a_T) = 2.254$ MPa) could be obtained from Fig. 1, and the shift factor ($\log a_T = -0.94$) could be obtained from Fig. 2. From the finite element simulation to the HTPB propellant, the maximum principal stress is 0.171 MPa, the maximum shear stress is 0.081 MPa, the maximum principal strain is 4.51%, and the critical area is located at the inner bore free surface of solid propellant grains. Using the time–temperature shift principle, the reciprocal value of the reduced strain rate could be calculated ($\log(1/R) = +7.53$). Inserting the value of $\log(1/R)$ in Fig. 4, the value of $\varepsilon_{\text{measured,max}}(t^*/a_T)$ could be found. From Eq. (5), the maximum allowable strain could be calculated ($\varepsilon_{\text{allowable,max}} = 18.0\%$). Then, inserting the value of $\varepsilon_{\text{allowable,max}}$ in Eq. (7), the factor of safety or damage fraction with respect to strain result under this thermal load step could be calculated:

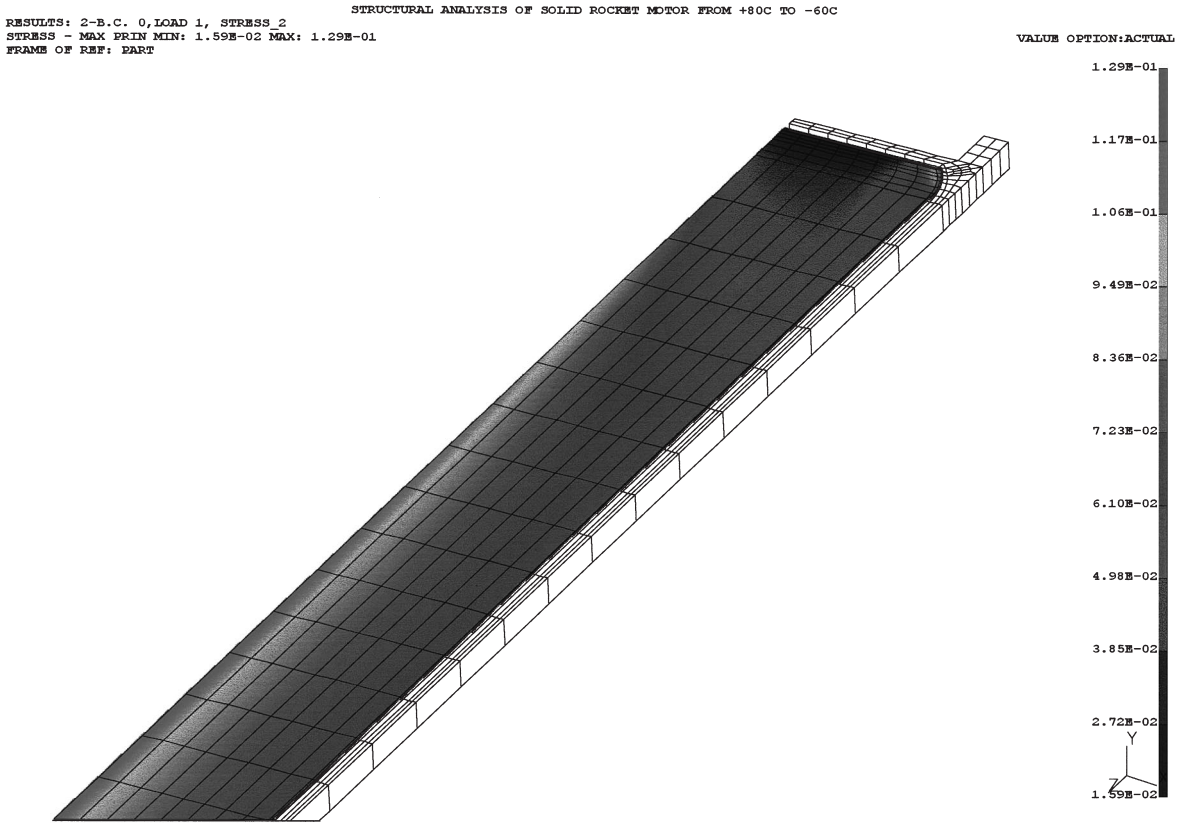

Fig. 8. The maximum principal stress distribution of the HTPB propellant under thermal loading history assumption 1 case.

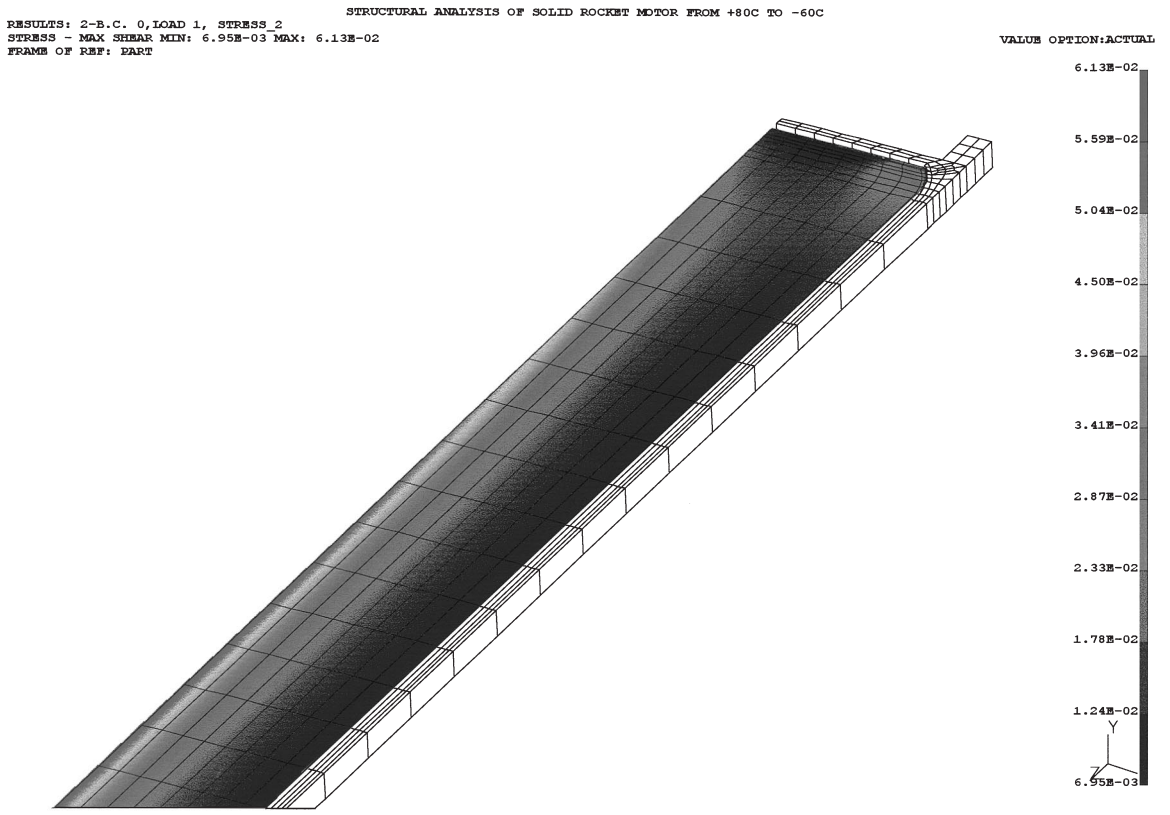

Fig. 9. The maximum shear stress distribution of the HTPB propellant under thermal loading history assumption 1 case.

$$\mathrm{SF}_{\varepsilon,\Delta T1} = 1/D_{\varepsilon,\Delta T1} = \varepsilon_{\mathrm{allowable,max}}/\varepsilon_{\mathrm{max},\Delta T1} = 3.991 = 1/0.251. \quad (11)$$

$$\mathrm{SF}_{\varepsilon,\Delta T2} = 1/D_{\varepsilon,\Delta T2} = \varepsilon_{\mathrm{allowable,max}}/\varepsilon_{\mathrm{max},\Delta T2} = 3.237 = 1/0.309. \quad (12)$$

4.2.2. The load step from $T_{storage} = +25°C$ to $T_{firing} = -60°C$

Under this thermal loading condition, the design load is defined as $T_{\mathrm{design}} = -85°\mathrm{C}$. The effective propellant modulus ($E(t^*/a_T) = 5.390$ MPa) could be obtained from Fig. 1, and the shift factor ($\log a_T = +1.66$) could be obtained from Fig. 2. From the finite element simulation to the HTPB propellant, the maximum principal stress is 0.765 MPa, the maximum shear stress is 0.365 MPa, the maximum principal strain is 6.95%, and the critical area is located at the inner bore free surface of solid propellant grains. Using the time–temperature shift principle, the reciprocal value of the reduced strain rate could be calculated ($\log(1/R) = +2.62$). Inserting the value of $\log(1/R)$ in Fig. 4, the value of $\varepsilon_{\mathrm{measured,max}}(t^*/a_T)$ could be found. From Eq. (5), the maximum allowable strain could be calculated ($\varepsilon_{\mathrm{allowable,max}} = 22.5\%$). Then, inserting the value of $\varepsilon_{\mathrm{allowable,max}}$ in Eq. (7), the factor of safety or damage fraction with respect to the strain result under this load step could be calculated.

4.2.3. Factor of safety or damage fraction under thermal loading history assumption 2

Using Eq. (8), the final factor of safety or damage fraction, located at the inner bore-free surface of the HTPB propellant could be calculated from the results of Eqs. (11) and (12).

$$(1/\mathrm{SF})_{\varepsilon} = D_{\varepsilon} = \sum D_{i,\varepsilon} = D_{\varepsilon,\Delta T1} + D_{\varepsilon,\Delta T2} = 0.560 = 1/1.786. \quad (13)$$

4.3. Thermal loading history assumption 3

This is similar to the analysis procedure of thermal loading history assumption 2, but with five thermal load steps from curing to storage and five thermal load steps from storage to firing, and totally 10 thermal load steps along the total thermal loading history. Finally, the factor of safety or damage fraction located at the inner bore-free surface of the HTPB propellant could be calculated:

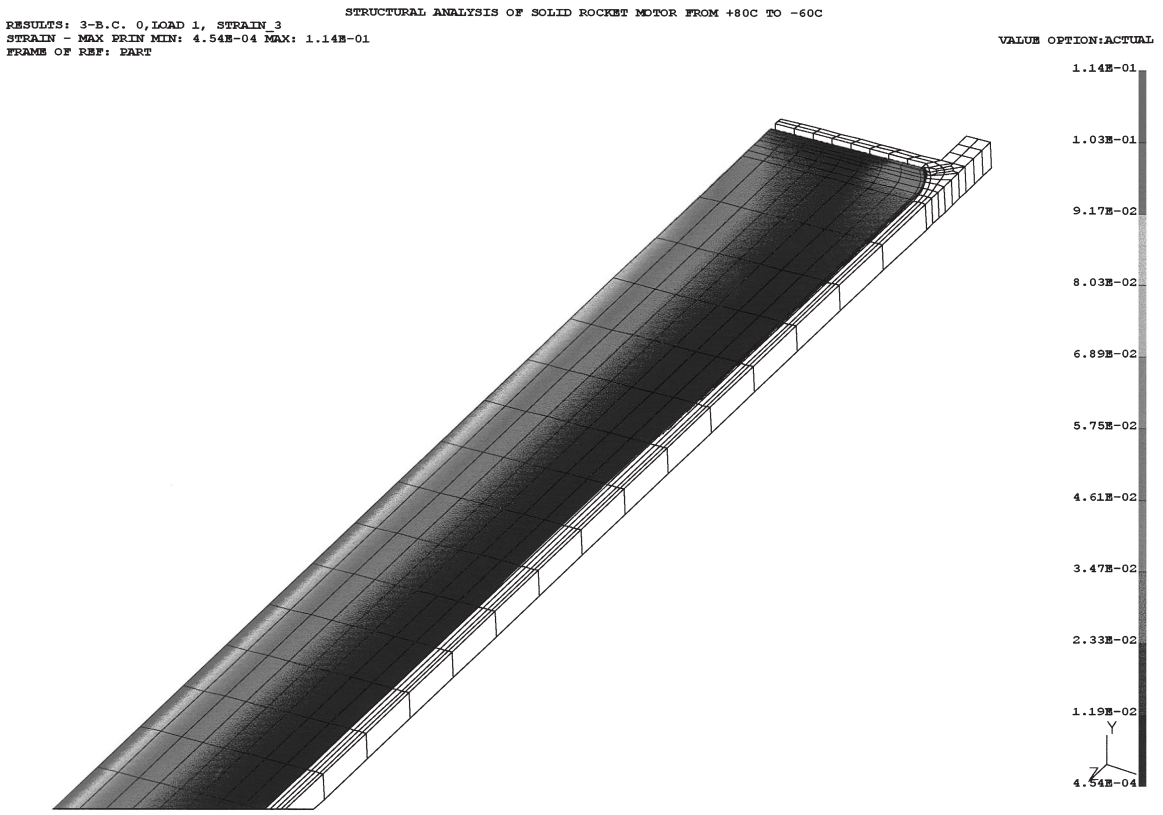

Fig. 10. The maximum principal strain distribution of the HTPB propellant under thermal loading history assumption 1 case.

$$(1/\mathrm{SF})_{\varepsilon} = D_{\varepsilon} = \sum D_{i,\varepsilon} = D_{\varepsilon,\Delta T1} + D_{\varepsilon,\Delta T2} + \cdots + D_{\varepsilon,\Delta T9} + D_{\varepsilon,\Delta T10} = 0.575 = 1/1.738. \quad (14)$$

4.4. Thermal loading history assumption 4

This is similar to the analysis procedure of thermal loading history assumption 2, but with 10 thermal load steps from curing to storage and 10 thermal load steps from storage to firing, and totally 20 thermal load steps along the total thermal loading history. Finally, the factor of safety or damage fraction located at the inner bore-free surface of HTPB propellant could be calculated:

$$(1/\mathrm{SF})_{\varepsilon} = D_{\varepsilon} = \sum D_{i,\varepsilon} = D_{\varepsilon,\Delta T1} + D_{\varepsilon,\Delta T2} + \cdots + D_{\varepsilon,\Delta T19} + D_{\varepsilon,\Delta T20} = 0.576 = 1/1.737. \quad (15)$$

4.5. Thermal loading history assumption 5

This is similar to the analysis procedure of thermal loading history assumption 2, but with 20 thermal load steps from curing to storage and 20 thermal load steps from storage to firing, and totally 40 thermal load steps along the total thermal loading history. Finally, the factor of safety or damage fraction located at the inner bore free surface of the HTPB propellant could be calculated:

$$(1/\mathrm{SF})_{\varepsilon} = D_{\varepsilon} = \sum D_{i,\varepsilon} = D_{\varepsilon,\Delta T1} + D_{\varepsilon,\Delta T2} + \cdots + D_{\varepsilon,\Delta T39} + D_{\varepsilon,\Delta T40} = 0.576 = 1/1.737. \quad (16)$$

5. Results and discussion

(1) From the results analyzed by thermal loading history assumption 1 (SF = 2.175), thermal loading history assumption 2 (SF = 1.786), thermal loading history assumption 3 (SF = 1.738), thermal loading history assumption 4 (SF = 1.737) and thermal loading history assumption 5 (SF = 1.737), diverse thermal loading history assumption could obtain different result (Fig. 11) and improper simplification (e.g.: thermal loading history assumption 1) used in the past literature, would result in a unconservative factor of safety or damage fraction to evaluate the structural integrity of solid rocket motor. Therefore, the thermal loading history

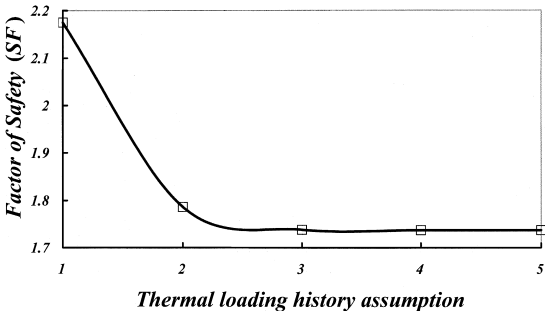

Fig. 11. The factor of safety for the HTPB propellant under diverse thermal loading history assumption.

assumption plays a very important role in the structure designed by viscoelastic material.

(2) In general, the critical location under the ignition pressurization loading case is at the interface between the outer case and the inner HTPB propellant, and the critical location under thermal loading case is at the inner bore free surface of solid propellant grains. While using the cumulative damage theory to calculate the factor of safety or the damage fraction of the HTPB propellant, the superposition task needs to be implemented under the restriction of the same critical location. Therefore, the most critical analytical results from pressure loading and thermal loading cases could not superpose directly because their critical locations are different. Because the main aim of this article is to study the thermal loading history effect under diverse thermal loading history assumption, and the maximum principal strain of inner bore-free surface of solid propellant grains was chosen to be analyzed and discussed.

(3) For a long time period of storage under variation temperature environment, the physical parameters of HTPB propellant would be affected by chemical aging, and the thermal loading effect would be more important. Therefore, an appropriate thermal loading history assumption, accompanied by an effective chemical aging model could be used to evaluate the storage life of a solid rocket motor reasonably. In addition, for the flight dynamic loading case of air-to-air missile system, the accumulative damage model developed by Bills [2] could be adopted to deal with the mechanical aging problem of solid propellant grains.

(4) Because the configuration of a solid rocket motor is too complex to predict the critical area and failure mode in the design phase, using a simple analytical model, the finite element simulation becomes the best method to obtain the stress distribution under diverse loading cases. Without the numerical analysis, designers need much more time to try and error to get a feasible design type accompanied by many experimental data. Therefore, the finite element analysis can reduce the project span time and save the total project cost.

6. Conclusions

An elaborate and extensive structural analysis of solid propellant grains, considering the thermal loading history effect was carried out using a commercial analysis FEA software package [24,25] with a CAE pre-post processor [26]. A 3D solid model was adopted to obtain detailed analysis results. In order to simulate the time–temperature-dependent behavior of incompressible and thermoviscoelastic polymer materials, concepts of time–temperature shift principle, cumulative damage theory and reduced integration were used. In addition, five diverse types of thermal loading history assumption were performed for discussing the thermal loading history effect. Results show that the thermal loading history effect is important for structural integrity of the solid propellant grains and improper negligence may cause structural failure of solid rocket motor system. The structural analysis highlighted several areas of interest. Recommendations resulting from this work have been forwarded to the designer, for incorporation of modification, and to other appropriate areas for design evaluation.

References

[1] Svob GJ, Bills Jr. KW. Predictive surveillance technique for air-launched rocket motors. J Spacecraft 1984;21(2):162–7.

[2] Bills Jr. KW. Structural design nomograph for thermal cycling of tactical rocket propellants. NWC Tech Memo 3365, 1977.

[3] Chyuan S-W. Life assessment of solid-propellant structure under thermal cycling (structure over test) using structural design nomograph. Proceedings of the Fifth ROC Symposium on Fracture Science, 1998. p. 31–8 [in Chinese].

[4] Christiansen AG, Layton LH, Carpenter RL. HTPB propellant aging. J Spacecraft 1981;18(3):211–5.

[5] Chang WM, Chyuan SW, Shieh NC. Aging life prediction of polymer material structure using MSC/NASTRAN and layton equation. MSC Taiwan Users' Conference Proceedings, 1994 [in Chinese].

[6] Chyuan S-W. Finite element simulation on solid-propellant structure under thermal shock loads. Proceedings of the 14th National Conference on Mechanical Engineering, The Chinese Society of Mechanical Engineers, P100-107 Chung-Li, Taoyuan, Taiwan, ROC, 1997 [in Chinese].

[7] Chen JT, Leu S-Y. Finite element analysis, design and experiment on solid propellant motors with a stress reliever. Finite Elem Anal Des 1998;29:75–86.

[8] Solid propellant grain structural integrity analysis. NASA SP 8073, 1973.

[9] Lin SL, Tsai IC, Shieh NC. MSC/NASTRAN stress analysis application in linear viscoelastic material problem.

MSC Taiwan Users' Conference Proceedings, 1989 [in Chinese].
[10] Chyuan S-W. Modeling and analysis of solid-propellant viscoelastic structure on air-to-air missile. Proceedings of the Fifth National Conference on Science and Technology of National Defense, ROC, 1996. p. 515–22 [in Chinese].
[11] Jana MK, Renganathan K, Venkateswara Rao G. A method of non-linear viscoelastic analysis of solid propellant grains for pressure load. Comput Struct 1994; 52(1):61–7.
[12] Miner MA. Cumulative damage in fatigue. J Appl Mech, vol. 12, Trans. ASME, vol. 67, 1945. p. A159–64.
[13] Chyuan S-W. Structural analysis of solid-propellant using cumulative damage theory and MSC/NASTRAN. MSC Taiwan Users' Conference Proceedings, 1996 [in Chinese].
[14] Zienkiewicz OC, Morgan K. Finite elements and approximation. Swansea: Pineridge Press, 1983.
[15] Bathe KJ. Finite element procedures in engineering analysis. Englewood Cliffs, NJ: Prentice-Hall, 1982.
[16] Brebbia CA, Telles JCF, Wrobel LC. Boundary element techniques. Berlin: Springer, 1984.
[17] Chen JT, Hong H-K, Chyuan SW. Boundary element analysis and design in seepage problems using dual integral formulation. Finite Elem Anal Des 1994;17:1–20.
[18] Chyuan S-W. Finite element simulation of a Twin-Cam 16-valve cylinder structure. Finite Elem Anal Des, in press.
[19] Chyuan S-W, Chiou CY. Application and modeling of finite element method on structural mechanics and thermal analysis. Abstracts of Invited Lectures and Short Communications Delivered at the Sixth International Colloquium on Numerical Analysis and Computer Science with Applications, Plovdiv, Bulgaria, 1997. p. 31–3.
[20] William ML. Structural analysis of viscoelastic materials. AIAA J 1964;5:785–808.
[21] Findley WN, Lai JS, Onoran K. Creep and relaxation of nonlinear viscoelastic materials. Amsterdam: North-Holland, 1976.
[22] Morland LW, Lee EH. Stress analysis of linear viscoelastic materials with temperature variation. Trans Soc Rheo 1960;4:233–63.
[23] Minimum standard structural analysis procedures for solid rocket grains under thermal and pressurization loading. JANNAF Solid Propellant Structural Integrity Handbook, CPIA Publication no. 230, 1987.
[24] Schaeffer HG. MSC/NASTRAN primer: static and normal modes. Schaeffer Analysis, 1982.
[25] Chen JT, Lin SL, Chiou CY, Chyuan SW, Hwang JY, Harn WR, Chin WT. Finite element analysis and engineering applications using MSC/NASTRAN. Northern Gate Publication, Taipei, Taiwan, 1996 [in Chinese].
[26] I-DEAS User's Guide, Finite Element Modeling, SDRC, 1990.